*Metallophysics and Advanced Technologies*
*Металофіз. новітні технол.*
*Metallofiz. Noveishie Tekhnol.*
2025, vol. 47, No. 8, pp. 891–906
https://doi.org/10.15407/mfint.47.08.0891
Reprints available directly from the publisher



PACS numbers: 61.43.Gt, 61.72.Dd, 61.72.Ff, 81.05.Bx, 81.20.Ev, 81.20.Hy, 83.50.Uv

# The Potential of Titanium-Alloys' Manufacturing with Metal Injection Moulding Approach Using Various Powder Feedstocks

O. M. Ivasishin, D. G. Savvakin, O. D. Rud, D. V. Oryshych, I. M. Kirian, A. M. Lakhnik, V. I. Bondarchuk, B. Kronowetter*, Yu. I. Torba**, and V. G. Manzhos**

*G. V. Kurdyumov Institute for Metal Physics, NAS of Ukraine,*
*36 Academician Vernadsky Blvd.,*
*UA-03142 Kyiv, Ukraine*
**KRONOWETTER Kunststoff- und Metalltechnik GmbH,*
*32 Gewerbestrasse,*
*D-83404 Mitterfelden, Germany*
***JSC 'Ivchenko-Progress',*
*2 Ivanova Str.,*
*UA-69068 Zaporizhzhia, Ukraine*

Two types of powder feedstocks based on pre-alloyed Ti–6Al–4V powder and blend of $TiH_2$ + Al–V powders (Ti–3Al–2V total composition) are comparatively studied to evaluate the conditions ensuring formation of promising microstructure and characteristics of titanium-alloy products with the metal-injection moulding (MIM) approach. Microstructure evolution on feedstock-compaction stage, debinding and vacuum sintering of powder compacts is studied to determine main features of powder-compact transformation into bulk titanium alloys. Sintering of debinded powders starts at 800°C; dehydrogenated $TiH_2$-based compacts demonstrate more active sintering owing to useful effect of hydrogen as temporary alloying element. Similar nearly dense (6% pores) and uniform alloy microstructure is formed in the depth of

Corresponding author: Orest Mykhaylovych Ivasishin
E-mail: ivas@imp.kiev.ua

Citation: O. M. Ivasishin, D. G. Savvakin, O. D. Rud, D. V. Oryshych, I. M. Kirian, A. M. Lakhnik, V. I. Bondarchuk, B. Kronowetter, Yu. I. Torba, and V. G. Manzhos, The Potential of Titanium-Alloys' Manufacturing with Metal Injection Moulding Approach Using Various Powder Feedstocks, *Metallofiz. Noveishie Tekhnol.*, **47**, No. 8: 891–906 (2025). DOI: 10.15407/mfint.47.08.0891

both sintered-powder compacts, while surface layers contain disperse Ti–O–C titanium-oxycarbide particles due to reaction of titanium matrix and binder remnants. Despite presence of oxycarbides useful for improvement of surface hardness and wear resistance, it suggests optimization of debinding regimes. Hardness values of sintered alloys (of 304–308 *HV*) allow recommendation of MIM approach as promising one for manufacturing titanium-based products possessing sufficient mechanical characteristics.

**Key words:** metal injection moulding (MIM), titanium alloys, powder, binder, sintering, microstructure, mechanical properties.

Леґований порошок складу Ti–6Al–4V та суміш порошків $TiH_2$ + Al–V (складу Ti–3Al–2V) було порівняльно досліджено з метою оцінки умов, що забезпечать формування гідної мікроструктури та характеристик титанових виробів за технологією інжекційного формування порошків. Досліджено еволюцію мікроструктури на стадіях компактування порошків із органічною зв'язкою, видалення зв'язки та вакуумного спікання порошкових компактів під час їхнього перетворення в масивні титанові стопи. Після видалення зв'язки спікання порошків розпочинається за температури у 800°C; водночас заготовки на основі гідриду Титану $TiH_2$ після дегідрування демонструють більш активне спікання завдяки корисному впливу Гідроґену як тимчасового леґувального елементу. Стопи із схожою однорідною мікроструктурою та малим вмістом залишкових пор (6%) сформовано в об'ємі обох спечених порошкових заготівок, в той час як їхні поверхневі шари містили дисперсні частинки оксикарбідів Ti–O–C, що утворилися в результаті реакції залишків зв'язки та титанової матриці. Присутність оксикарбідів є корисною для підвищення поверхневої твердости та показників стійкости щодо зношування; проте, це вимагає оптимізації режимів видалення зв'язки. Твердість спечених стопів (304–308 *HV*) уможливлює рекомендувати технологічні підходи на основі інжекційного формування металевих порошків для одержання титанових виробів з достатніми механічними характеристиками.

**Ключові слова:** технологія інжекційного формування металевих порошків (MIM), титанові стопи, порошок, зв'язка, спікання, мікроструктура, механічні характеристики.

*(Received 16 June, 2025; in final version, 1 July, 2025)*

## 1. INTRODUCTION

The titanium alloys are attractive materials for wide application in aerospace, machinery, oil industries and medicine owing to high strength-to-weight ratio and excellent corrosion resistance [1, 2]. Titanium alloys are used for manufacturing gas turbine components (blades, discs) serving at temperatures up to 600–650°C, fasteners and other critical and not critical components. However, excessive cost of titanium restricts its practice application and forces development of advanced cost-efficient manufacturing technologies for titanium-

based alloys and products of them. The manufacturing approaches should ensure not only sufficient cost-efficiency of the processing, but also achievement of required microstructure, mechanical, service characteristics and high shape accuracy of titanium products, which is challenging and extremely important target.

Contrary to conventional multistep manufacturing processes based on casting, hot deformation of alloy ingots and machining with significant material losses, the net-shape manufacturing technologies based on powder metallurgy ensure cost-efficiency owing to reduction of material waste and avoidance of complicated processing steps [2]. Metal-injection moulding (MIM) powder technology [3–5] is promising to reduce the processing cost and to achieve sufficient product characteristics that was proved by wide net-shape production of stainless steel and ceramic products. MIM approach is based on relatively simple set of operations, including mixing metal powders and organic binders to create feedstock granules, heating powder + binder feedstocks to achieve sufficient fluidity and forming at low pressures (20–150 MPa) into net-shape workpieces, subsequent binder removal and sintering of the powders to obtain final products of desirable shape.

Despite significant progress in MIM processing for other materials, MIM production of titanium alloys faces problematic issues. On heating of titanium-based MIM powder compacts, organic binder should be completely removed from compacts before temperatures at which sintering activates. Otherwise, binder remnants react with activated titanium surface contaminating metal with oxygen, carbon and other impurities, forming brittle titanium carbide phase [2], and hindering densification, thus, leading to degradation of mechanical characteristics. After debinding completion and before sintering development, adhesion forces between powder particles become weak, creating risk for powder compact destruction. At higher temperatures, activated sintering should ensure transformation of powder particles into bulk nearly-dense and uniform microstructure with minimal impurity content, which, in turn, provide sufficient mechanical characteristics. For the reasons above, development of proper debinding and sintering conditions for titanium-based MIM compacts is challenging task.

Conventional die-pressing and sintering powder technology is alternative method for production titanium-based materials of relatively simple geometrical shape. Compared to MIM powder method, die-pressing and sintering one uses noticeably higher compaction pressure values (200–600 MPa and even more), allowing successful powder compaction even without binder at room temperature. Despite noticeably different conditions for MIM feedstock compaction and die-pressing of metal powders, powder + binder MIM feedstock can be also compacted with die-pressing. Die-compacted titanium-based feedstocks can be used as model samples to investigate main features of

MIM process, which occurs during heating, debinding, sintering of powder compacts and microstructure evolution.

High fluidity of disperse spherical powder particles determines their wide use in MIM technologies [3–5]. For this reason, gas-atomized pre-alloyed powders of spherical shape are the most attractive raw materials. On the another hand, titanium-hydride $TiH_2$ powder of irregular shape and powder blends on its base demonstrated significant advantages compared to conventional (not hydrogenated) titanium powders in simplest press-and-sinter manufacturing technology [2, 6, 7]. In hydrogenated powder approach, hydrogen is temporary alloying element for titanium and emitted from metal on vacuum heating, ensuring activated sintering and enhanced characteristics of sintered products at noticeably improved cost-efficiency. Therefore, comparative study of MIM feedstocks based on either spherical pre-alloyed titanium powder or blend of irregular $TiH_2$ and alloying powders is of great interest.

The aim of the study was comparative investigation of main features of compaction, debinding and sintering powder feedstocks based on various titanium powders to determine the conditions ensuring formation of promising microstructure and characteristics of titanium alloy materials with the MIM approach.

## 2. MATERIALS AND EXPERIMENTAL PROCEDURE

Two titanium-based powder compositions were selected for investigation. The first one was industrially produced pre-alloyed Ti–6Al–4V (% wt.) spherical powder (less than 30 μm in size). The second one was powder blend of Ti–3Al–2V (% wt.) total composition consisted of irregular $TiH_2$ titanium hydride (less than 63 μm) and alloying 60% Al–40% V (less than 40 μm) master alloy powders (hereafter, blend is designated as $TiH_2 + 3Al–2V$). The first composition is the most widely used titanium alloy over the world. Because of Ti–6Al–4V alloy possessing sufficiently-high strength level ($UTS = 950$ MPa, elongation 10% [8]), the Ti–3Al–2V one was selected for testing as material providing some lower strength but better ductile characteristics and taking into consideration better cost-efficiency. Comparative study of two noted powder compacts at all MIM processing stages allows determination of hydrogen effect on material (either hydrogenated $TiH_2$ or non-hydrogenated conventional titanium powders), powder shape (either spherical or irregular one) as well as pre-alloyed and blended elemental powder approaches in compaction, debinding and sintering stages to select promising MIM processing options.

Each powder composition was mixed with PolyMIM [9] organic binder to obtain powder-binder feedstock granules of about 3 mm in size. The feedstock granules were compacted at 620 MPa in steel die to

form compacts 10 mm in diameter and 10–12 mm in height. The feedstock compacts were debinded in two steps: preliminary debinding was implemented in hot water at 70°C for 30 hours, then compacts were put in vacuum furnace and heated (rate of 5°C/min) to 800°C with 2 hours isothermal exposure for final debinding step. After that, heating was continued; compacts were sintered at 1250°C for 3 hours, and cooled in the furnace. For investigations of microstructure evolution at intermediate heating steps, some compacts were cooled immediately after 800°C, 2 hours exposure, and after subsequent heating up to 900°C. To evaluate the influence of heating regime on debinding and development of powder sintering, selected compact was heated 5°C/min up to 900°C without exposure at 800°C and immediately cooled.

The microstructure of samples at all processing steps was studied using scanning electron microscopy (SEM, TESCAN Vega III, equipped with Brucker EDX analyser to determine local chemical composition of material, including powder surface contamination with binder remnants). Polished surfaces of sintered alloys were also studied with light optical microscopy (Olympus IX 70) using etching with Kroll's reagent (2% $HF + 5\%$ $HNO_3 + 92\%$ $H_2O$) to reveal microstructure. The phase composition of green feedstock compacts and final sintered products was investigated with x-ray diffraction using Mo anode. The density of compacts was evaluated with precise measuring their geometrical sizes and mass, while the mass loss of samples at each processing steps was measured to evaluate the debinding degree. Finally, the density of sintered materials was determined with Archimedes' technique. For preliminary evaluation of mechanical properties of sintered materials, Vickers hardness measurements were performed using Wolpert 432 SVD testing machine.

## 3. RESULTS AND DISCUSSION

The microstructures of green compacted feedstocks are presented in Fig. 1. Not quite uniform redistribution of powder particles and binder within the compacts of both types was observed (Fig. 1, *a*, *b*). Both spherical and irregular powder particles were not closely arranged at compaction stage, leaving the voids between particles and thin pore channels densely filled with binder. The surface of all particles is covered with binder at sufficient adhesion between binder and surfaces (Fig. 1, *c*, *d*). The density of Ti–6Al–4V green compacts was 2.75 g/cm$^3$ due to considerable volume part of lightweight binder in the compact. For $TiH_2 + 3$Al–2V powder blend, the density of compacts was even lower (2.18 g/cm$^3$) due to lower density of titanium hydride (3.9 g/cm$^3$) versus density of Ti–6Al–4V alloy (4.43 g/cm$^3$). Used compacting pressure value (620 MPa) was not high enough for considerable deformation of hardened gas atomized Ti–6Al–4V powder particles (Fig. 1,

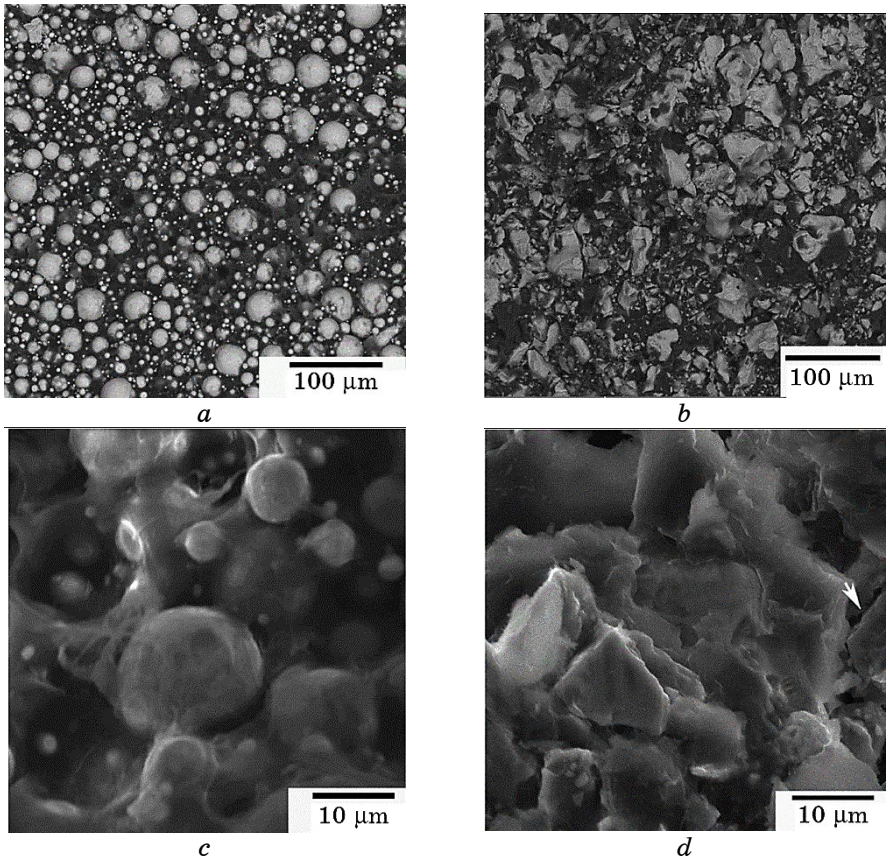


**Fig. 1**. Microstructure of green feedstock compacts: Ti–6Al–4V (*a*, *c*), $TiH_2$ + 3Al–2V (*b*, *d*). Crack in $TiH_2$ particle is shown by arrow in (*d*).

*c*); however, traces of deformation were observed at some contacts between particles. Contrary, cracking of brittle and low-strength $TiH_2$ particles with formation of fine irregular fragments was observed (Fig. 1, *b*, *d*) for corresponding green compacts.

X-ray diffraction (XRD) analysis was conducted for both 'green' feedstock compacts of Ti–6Al–4V alloy and $TiH_2$ + 3Al–2V powder mixture (Fig. 2, *a*, curve *1* and Fig. 2, *b*, curve *1*, respectively). The diffraction pattern of the Ti–6Al–4V-based sample (Fig. 2, *a*, curve *1*) shows characteristic peaks corresponding to the either h.c.p. α- or α′-martensite phase, while diffraction peaks of b.c.c. β-phase were not detected. This result suggests that metastable single-phase α′ martensite condition was formed instead of stable α + β phase condition for Ti–6Al–4V powder during fast cooling on gas atomization manufacturing process. The diffraction pattern of the $TiH_2$-based sample (Fig.

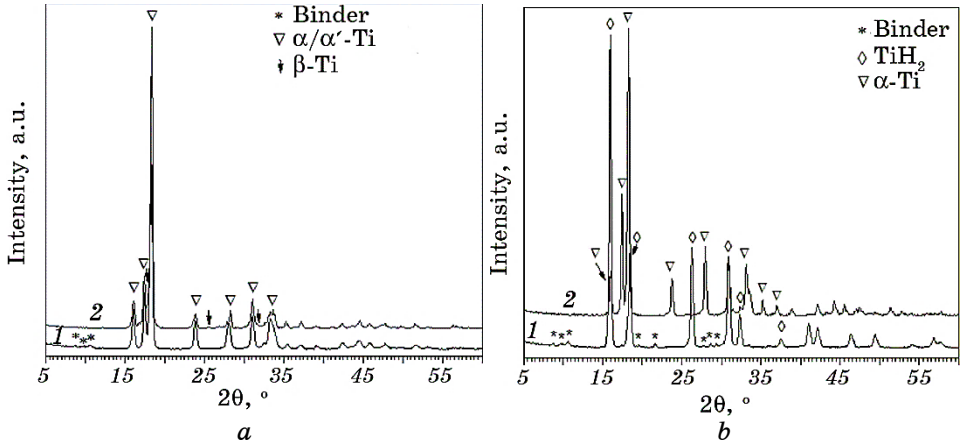


**Fig. 2.** XRD patterns of Ti–6Al–4V (*a*) and $TiH_2$ + 3Al–2V (*b*) feedstock samples in initial compacted condition (*1*) and after debinding and sintering at 1250°C for 3 hours (*2*).

2, *b*, curve *1*) shows distinct peaks corresponding to titanium hydride ($TiH_2$), while peaks corresponding to Al–V-master alloy powder were not detected due to low amount of this powder in the mixture. Traces of binder were also observed for both compacted feedstock samples. So, the XRD analysis indicates the typical phase composition of the raw powders and their structural stability after forming green compacts. The absence of new phases or reaction products suggests that the powder materials remain stable during the early stages of processing. These results are crucial for subsequent control of the sintering process and for tailoring the final properties of the materials.

The first debinding stage (washing in hot water with removal of binder soluble components) resulted in appearance of caves between powder particles and their fragments (see Fig. 3). However, surface of particles is still covered by binder at this stage. Partial binder removal led to ≅ 5% mass loss for Ti–6Al–4V compact and 10–11% mass loss for titanium hydride-based compacts. Such difference in mass loss at first debinding stage can be explained with more intensive binder removal from $TiH_2$ + 3Al–2V compacts, obviously, due to more developed surface for irregular $TiH_2$ particles and their finer fragments, and, hence, better water penetration in caves and channels between irregular fragments.

Subsequent vacuum heating up to 800°C with 2 hours isothermal exposure led to noticeable changes in microstructure of both compacts (Fig. 4, *a*, *b*) due to final debinding, dehydrogenation of titanium hydride and sintering beginning within noted temperature range. After vacuum debinding stage, binder remnants were not observed between

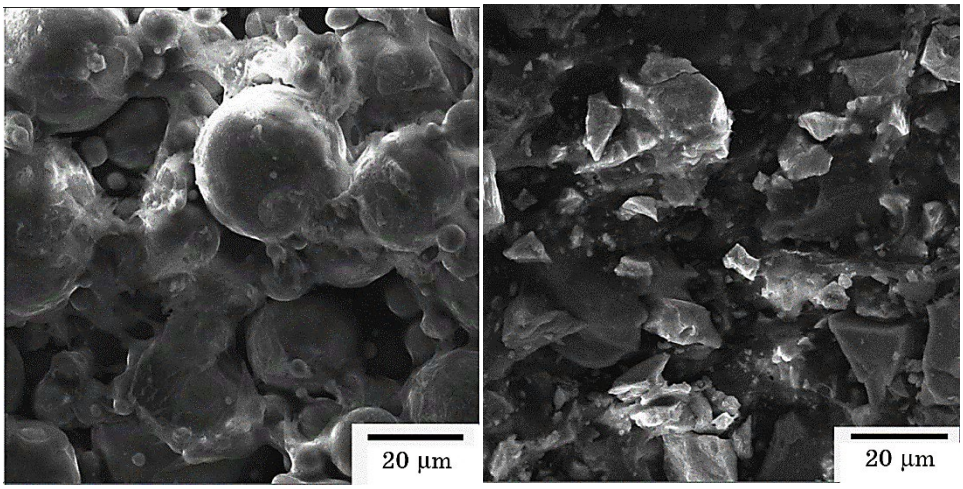


**Fig. 3.** Microstructure of compacts after first debinding stage (washing in hot water): Ti–6Al–4V (*a*), $TiH_2$ + 3Al–2V feedstock (*b*).

powder particles, while carbon content up to 2.1% (wt.) was still detected at the cleaned particle surfaces (Table 1). The mass loss increased to 11.2% for Ti–6Al–4V powder compared to corresponding green feedstock, while for $TiH_2$ + 3Al–2V powder blend mass loss achieved 22% due to debinding development and emission of 3–4% (wt.) hydrogen on $TiH_2 \rightarrow Ti + H_2$ (gas) transformation.

At this heating stage, obvious features of sintering beginning are revealed. Sintering necks are formed between spherical Ti–6Al–4V particles (Fig. 4, *a*), while formation of necks and smoothing of surface relief (Fig. 4, *b*) for irregular dehydrogenated titanium particles are observed. Sintering processes were developed even more intensive during subsequent heating up to 900°C (Fig. 4, *c*, *d*). Sintering development at 800–900°C ensures appearance of sufficient bonding forces between particles and, hence, improved strength of compacts. Crushing of compacts allows observation of fractured necks between particles, traces of fractured necks are especially visible at smooth surfaces of spherical particles (Fig. 4, *a*, *c*). Densification and shrinkage of dehydrogenated compacts (Fig. 4, *b*) became clearly observed at this heating stage, despite porous channels between particles still presented. Contrary, densification and shrinkage of Ti–6Al–4V powder compacts was slightly developed (Fig. 4, *a*). Since sintering beginning stage and formation of necks between particles is controlled by surface diffusion, while volume diffusion is responsible for shrinkage and densification, it can be concluded activation of surface diffusion for Ti–6Al–4V powder and noticeable activation of both surface and volume diffu-

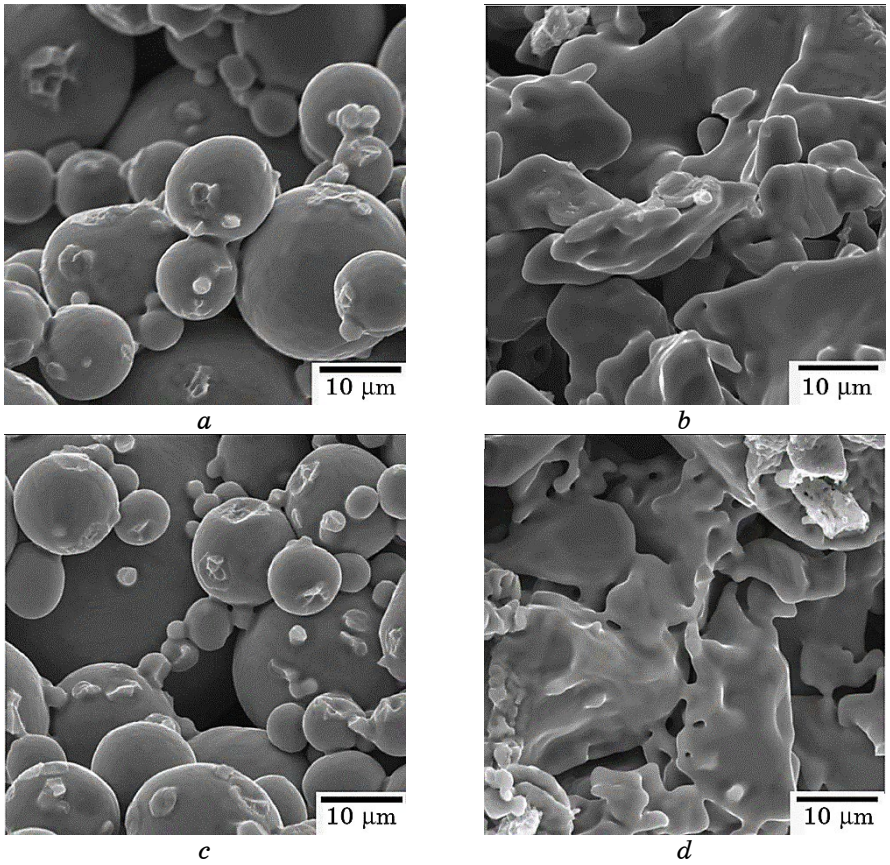


**Fig. 4.** Microstructure of Ti–6Al–4V (*a*, *c*) and $TiH_2 + 3Al–2V$ (*b*, *d*) powder compacts after debinding at 800°C, 2 hours (*a*, *b*) and subsequent heating to 900°C (*c*, *d*).

sion for dehydrogenated titanium powder before 800–900°C.

Average chemical composition of the powder surfaces at different debinding and heating stages was presented for analysis in Table 1. Despite significant variation in local element content at the powder surfaces detected with Brucker EDX analyser, data presented in Table 1 allow making general conclusion about debinding and surface processes for both pre-alloyed Ti–6Al–4V particles and $TiH_2 + 3Al–2V$ powder blend. Variation of measured values was caused with different thickness of binder layer preliminary covering the powder particles and different opportunities for binder evacuation through pore channels of various thicknesses.

Significant amount of binder remains at the particle surfaces after washing in hot water. Surfaces are characterized with high local con-

**TABLE 1**. Average values of element content at the surfaces of Ti–6Al–4V and $TiH_2$ (dehydrogenated Ti) powder particles at different processing steps (N/M—measured value is below error value/element was not detected).

| Element, % wt. | Ti–6Al–4V powder surface | | | $TiH_2$/dehydrogenated Ti powder surface | | | |
|---|---|---|---|---|---|---|---|
| | washed in hot water | 800°C, 2 hours exposure | 800°C, 2 hours exposure + heated to 900°C | washed in hot water | 800°C, 2 hours exposure | 800°C, 2 hours exposure + heated to 900°C | continuous heating to 900°C |
| Ti | balance | balance | balance | balance | balance | balance | balance |
| Al | 5.9 | 6.0 | 6.2 | 0.4 | 0.7 | 1.3 | 0.2 |
| V | 3.9 | 3.8 | 3.8 | N/M | N/M | 0.5 | N/M |
| C | 10.4 (up to 41.0) | 2.1 | 2.1 | 12.5 | 1.9 | 1.1 | 1.1 |
| O | 2.5 | 0.5 | N/M | 3.2 | N/M | N/M | 0.5 |

tent of carbon (average values are about of 10–12%, however, it achieves up to 41% in some locations due to thicker binder layers remaining at the surfaces) and oxygen (about of 3%). Relatively-slow vacuum heating used in present study (5°C/min) and 2 hours exposure at 800°C resulted in binder removal accompanied with noticeable reduction of carbon (2.1–1.9%) and oxygen (0.5% and even lower, being below error value) contents.

For $TiH_2$ + 3Al–2V powder blend, completed dehydrogenation of titanium hydride and hydrogen evacuation took place during heating to 800°C. Among particles of $TiH_2$ + 3Al–2V powder blend, surface composition of dehydrogenated titanium particles was investigated only (Table 1) due to relatively low amount of Al–V master alloy particles in the blend. Diffusion activation at 800–900°C, in addition to sintering beginning, led to redistribution of Al from Al–V master alloy particles and increase in Al content at the dehydrogenated titanium particles, while diffusion redistribution of vanadium is much slower and do not observed at 800°C. As expected, noticeable changes in Al and V content in pre-alloyed Ti–6Al–4V powder do not occur. All diffusion-controlled processes were less developed during continuous heating to 900°C (no exposure at 800°C); thus, some higher O content and lower Al content were detected at the surface of dehydrogenated Ti particles. Earlier investigation of both titanium and titanium-hydride powder surfaces [10] revealed that they demonstrate quite similar surface structures. Titanium oxide layers ($TiO_2$ and oxides with lower titanium oxidation degree $TiO_X$, $X < 2$) as well as absorbed atmospheric moisture ($H_2O$, OH groups) were detected on the surface. Current results suggest not only binder removal from the powder surfaces during vacuum

heating to 800–900°C. Sufficient contribution into decreased O content observed at these heating stages for surfaces of both Ti–6Al–4V and dehydrogenated $TiH_2$ powders (Table 1) was also caused with diffusion dissolution of surface oxides at high temperatures [2, 11]. It should be noted obvious advantage of titanium hydride powder, because of emission of atomic hydrogen promotes surface cleaning of dehydrogenated titanium particles [2, 10] and, thus, gives contribution into reduction of C and O contents compared to unhydrogenated Ti–6Al–4V powder at this heating stage (Table 1).

All described surface processes make contribution into activated sintering of powder particles already at 800°C (Fig. 4). Moreover, dehydrogenation of titanium hydride increases density of crystal defects in titanium, which accelerates volume diffusion providing more developed sintering and homogenization of Ti + 3Al–2V powder blend. As a result, bulk sintered and chemically uniform alloys were produced for both studied MIM compacts. Both sintered alloys (Fig. 5, *a*, *b*) demonstrated typical lamellar $\alpha + \beta$ microstructures with some coarser $\alpha$-phase lamellae (up to 20 μm thickness) for Ti–3Al–2V alloy due to lower content of alloying elements.

The XRD patterns of sintered samples (Fig. 2) show the complete disappearance of peaks corresponding to the organic binder, indicating its full removal during thermal processing for both materials. In the Ti–6Al–4V sample (Fig. 2, *a*, curve *2*), the diffraction peaks of the $\alpha$-phase of titanium and traces for $\beta$-phase peaks confirms transformation of initial martensite phase into stable $\alpha + \beta$ structure on sintering. The diffraction pattern of the $TiH_2$ + 3Al–2V material (Fig. 2, *b*, curve *2*) shows a complete disappearance of peaks corresponding to titanium hydride, while peaks of the $\alpha$-phase Ti appear confirming the entire release of hydrogen during sintering. Content of vanadium (2%) in the alloy is obviously too low to detect weak $\beta$-phase peaks in produced $\alpha + \beta$ structure. The results once more confirmed the feasibility of using $TiH_2$ as an alternative titanium source with controlled dehydrogenation.

Formation of bulk materials accompanied with significant shrinkage of powder compacts. Ti–6Al–4V compacts demonstrated 12% linear shrinkage due to sintering only, while linear shrinkage for $TiH_2$-based Ti–3Al–2V compacts achieved 18% owing to additional shrinkage of $TiH_2$ particles on dehydrogenation. The measured densities of sintered materials are 4.17 g/cm$^3$ for Ti–6Al–4V alloy and 4.18 g/cm$^3$ for Ti–3Al–2V alloy, which both correspond to approximately 6% of residual pores in materials. So, for both alloys, similar level of residual porosity and pores of similar sizes demonstrating close to spherical shape are observed. However, pores are not quite uniformly redistributed over the sintered materials. Noticeably-higher amount of pores was observed for surface and subsurface layers (Fig. 5, *c*, *d*) than for

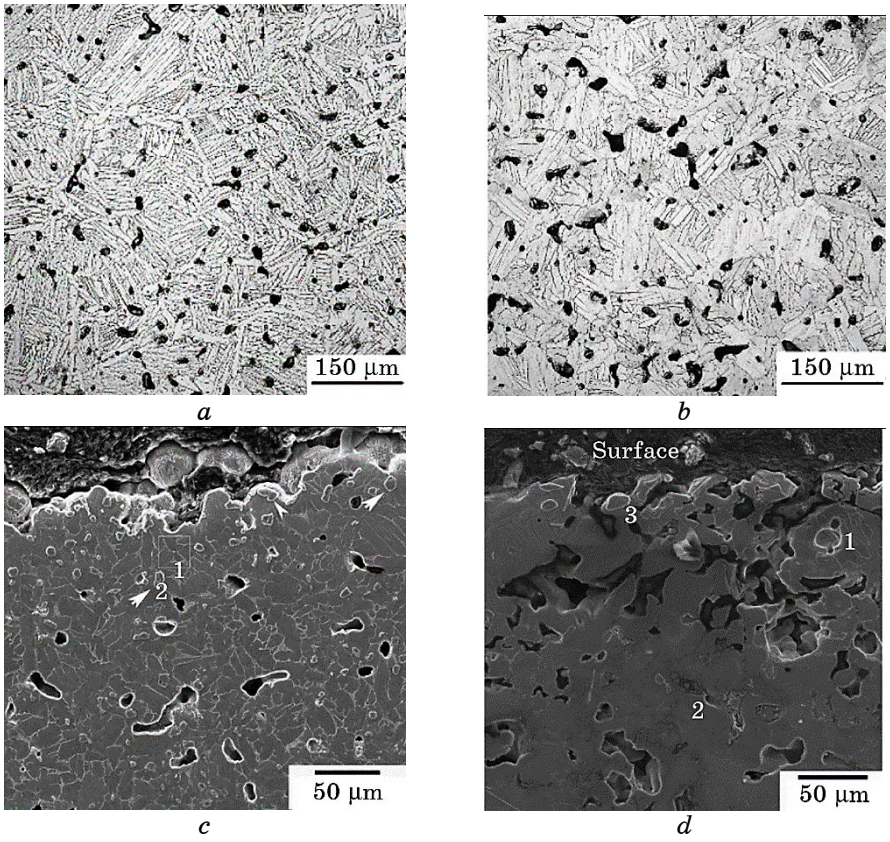


**Fig. 5.** Microstructure images (light optical microscopy) of sintered (1250°C, 3 hours) Ti–6Al–4V (*a*) and Ti–3Al–2V (*b*) alloys, as well as more detailed SEM images (*c*, *d*) of surface and subsurface layers of corresponding alloys. Ti–O–C particles are shown by arrows in (*c*), while points and areas used for local chemical analysis (see Table 2) are shown by numbers in (*c*, *d*).

nearly-dense compact depth; this tendency was especially manifested for Ti–3Al–2V material (Fig. 5, *d*).

Increased porosity observed within subsurface layers up to 200 μm in depth was explained with presence of binder remnants, which obviously negatively affect densification. Despite used EDX method does not allow reliable and accurate measurement of local carbon and oxygen contents at polished and etched alloy surfaces, it allows qualitative determination of the element distribution regularities. For both sintered alloys, increased content of carbon and oxygen (Table 2) as well as particles with especially-high content of noted impurities (identified as Ti–C–O titanium oxycarbides) were observed in subsurface layers 200–250 μm in depth (Fig. 5, *c*, *d*). At the same time, Ti–C–O precipitations

**TABLE 2.** Content of alloying elements and impurities (% wt.) measured in various locations at the polished and etched surfaces of sintered alloys (see Fig. 5, *c*, *d*).

| Element | Ti–6Al–4V (Fig. 5, *c*) | | | Ti–3Al–2V (Fig. 5, *d*) | | | |
|---|---|---|---|---|---|---|---|
| | Subsurface, area 1 | Subsurface, point 2 | Material volume | Subsurface, particle 1 | Subsurface, area 2 | Surface, particle 3 | Material volume |
| Al | 5.9 | 0.2 | 6.0 | 0.2 | 2.0 | 0.1 | 2.7 |
| V | 3.5 | 0.0 | 3.3 | 0 | 0 | 0 | 1.3 |
| C | 2.1 | 10.2 | 1.8 | 7.1 | 2.7 | 8.6 | 2.0 |
| O | 1.7 | 4.2 | 1.7 | 5.7 | 5.6 | 4.3 | 3.4 |

were not observed in deeper part of material volume at generally lower C and O contents detected in alloy matrixes. Oxygen content measured at polished and etched surfaces (Table 2) looks noticeably higher than real oxygen content in material volume due to surface preparation procedures and additional surface oxidation during polishing and etching. Higher content of oxygen measured at the polished Ti–3Al–2V alloy surface than for Ti–6Al–4V one (Table 2) is unexpected result, because of materials produced *via* hydrogenated powder approach usually are characterized with lower oxygen content. However, in present case, raw materials were produced with absolutely different methods, hence, contained different starting content of impurities.

Hardness measurements confirmed hypothesis about preservation of impurity content at admissible level in the depth of sintered alloys. Average hardness value within the volume of Ti–6Al–4V alloy was of 304 *HV* (individual values were within 289–320 *HV* in various locations), which is lower than hardness value for corresponding conventional material (342 *HV*) due to residual porosity. Average hardness for Ti–3Al–2V material volume was some higher: 308 *HV* (291–331 *HV*), this result can be explained with higher impurity content (O, C) despite lower content of alloying elements (aluminium and vanadium). Unfortunately, there was no possibility to measure the hardness of subsurface layer with Ti–O–C particles due to its low thickness. At the same time, the fact that volume hardness of both sintered materials with $\cong 6\%$ residual pores are quite below hardness value for conventional cast and wrought Ti–6Al–4V material means total content of all reinforcing impurities are close to those required by standards (O below 0.2%, C below 0.08%, N below 0.05%) and, hence, markedly lower than those detected on the surfaces (Table 2).

As important peculiarity of sintering process for both used MIM titanium compositions, it should be noted development of their sintering at relatively low temperatures (already at 800°C), which is noticeably lower then temperatures for sintering activation of nickel-based In-

conel 718 powder previously studied in similar MIM compacts [12]. Such difference in sintering activation temperature for titanium and nickel-based powders results from different processes occur at their surfaces, which, in turn, depends on stability of passivation surface oxide films and diffusion mobility of base elements. Titanium-based and titanium-hydride particles are covered with $TiO_2$ films [10, 11], which are barriers for diffusion and prevent sintering. On heating and diffusion activation, surface titanium oxides either dissolute at temperatures above 600°C [11] or can be reduced with atomic hydrogen emitted from the $TiH_2$ powder above 300–350°C [10]. Disappearance of surface titanium oxide layers for Ti–6Al–4V and dehydrogenated titanium particles owing to both noted reasons leads to surface activation with accelerated surface diffusion and formation of sintering necks between particles. Nickel surface is characterized with bilayer structure consisted of nickel hydroxide $Ni(OH)_2$ outer layer and oxide NiO inner layer [13]. For nickel-based Inconel-718 powder sintering was not developed up to 900°C and higher [12] suggesting the passivation effect of surface layer is more stable than for titanium. In addition, another reason for different sintering kinetic is difference in diffusion mobility of base elements: for example, self-diffusion of Ti is $10^{-17}$ $m^2 \cdot s^{-1}$ at 800°C [1], while this parameter for nickel is approximately one order of magnitude lower ($\cong 10^{-18}$ $m^2 \cdot s^{-1}$ at 800°C [14]).

Therefore, comparative analysis of results obtained for both types of model MIM samples suggests the MIM powder approach has promising potential for manufacturing titanium-alloy products using both blended elemental and pre-alloyed powders. Both spherical and irregular powder particles can be quite successfully used in press-and-sintering process to form comparable nearly-dense sintered microstructures with similar levels of residual porosity. Using hydrogenated powder ($TiH_2$ one in present study) obviously brings additional advantages into sintering and homogenization (if any) processes, namely, ensuring useful activation of diffusion in powder system at lower temperatures compared to conventional unhydrogenated titanium powder (Ti–6Al–4V one used in present study) (see Fig. 4). Following earlier results [2, 10], $TiH_2$ powder also promotes effective cleaning of powders with atomic hydrogen emitted on vacuum sintering. At the same time, using hydrogenated titanium led to higher shrinkage values of powder compacts that should be taken into consideration on product manufacturing.

Die-compaction at relatively high pressure (620 MPa) and subsequent sintering of both tested powder plus binder feedstocks ensure formation of low-porous uniform alloys with rather acceptable impurity content in the material depth, which follows from the obtained hardness characteristics comparable with hardness of conventional Ti–6Al–4V alloy. It is worth to note the presence of oxycarbide particles Ti–C–O in surface and subsurface layers of final alloy products, which

is consequence of the reaction of titanium and binder remnants at not optimized debinding conditions. Titanium-oxycarbide particles were formed on sintering either due to premature closing open porous channels between powder particles that prevents completed binder removing or due to deposition of volatile binder remnants on the compact surface in heated vacuum chamber. Despite Ti–C–O particles in alloy matrix are harmful for ductile characteristics, they create composite structure useful for higher strength–hardness characteristics of the surface and, hence, useful for wear resistance improvement. For the reasons above, optimization of debinding and sintering regimes is necessary in future to achieve set of mechanical characteristics required for each specific application.

No doubts, relatively-high compaction pressure (620 MPa) used in present experiments promotes reduction of porosity of green MIM compacts and final sintered products, as well as sufficient strength of powder compacts at all processing stages allowing easy handling even at the absence of binder. Classical MIM powder approach usually uses noticeably lower pressures (20–150 MPa) [3–5] but higher temperatures (up to 200°C) for feedstock compaction. Low compaction pressure results in higher shrinkage of compacts on sintering, which often is problematic issue. Moreover, at low compaction pressure when contacts between adjacent powder particles are less deformed and weakly bonded, there is a risk for fracture of powder compacts within 450–800°C interval, for which binder is already removed, but sintering not developed yet. The problem of compact fracture at intermediate processing stage was successfully overcome in present study for press-and-sintered titanium-based compacts. However, obviously, all noted problematic issues require further modification of debinding and sintering parameters to achieve nearly-dense net-shape titanium products with classic MIM approach.

## 4. CONCLUSIONS

1. MIM feedstocks based on spherical Ti–6Al–4V pre-alloyed powder and $TiH_2$ + Al–V irregular powder blend (corresponding to Ti–3Al–2V composition) with PolyMIM binder were comparatively studied in press-and-sinter approach to determine main features of MIM compact transformation into bulk titanium alloys.
2. Washing in hot water and subsequent vacuum heating ensured nearly completed debinding before 800°C, while sintering begun simultaneously at this temperature for both powder compacts. Dehydrogenation of $TiH_2$ powder led to more active sintering development for corresponding compacts at 800–900°C and higher shrinkage value (18%) than that for not hydrogenated Ti–6Al–4V powder (12%). In addition to accelerated sintering, raw hydrogenated powder is useful for reduc-

tion of impurity content in final alloy products.
3. Both types of used powders allow formation of similar nearly dense (6% pores) and uniform microstructure of titanium alloys. Surface layer of both sintered compacts contains disperse inclusions (up to 10–20 μm), which were identified as Ti–O–C titanium oxycarbides formed due to reactions of titanium matrix and binder remnants. Despite presence of oxycarbides is useful for improvement of surface characteristics (wear resistance, hardness), it suggests optimization of debinding regimes.
4. The hardness values (of 304–308 *HV*) of sintered alloys are comparable to the hardness of the conventional Ti–6Al–4V material that allows us to recommend the MIM method as promising for manufacturing titanium-based products with sufficient mechanical characteristics.

This work was supported by a grant No. 2023.04/0058 of the National Research Foundation of Ukraine.

## REFERENCES

1. G. Lutjering and J. C. Williams, *Titanium* (Springer: 2007).
2. *Titanium Powder Metallurgy: Science, Technology and Application* (Eds. Ma Qian and F. H. Froes) (Elsevier: 2015).
3. R. M. German, *Handbook of Metal Injection Molding* (Ed. D. F. Heaney) (Woodhead Publishing: 2012), p. 1.
4. F. T. Teferi and A. A. Tsegaw, *Advances of Science and Technology* (Ed. M. L. Berihun) (Springer: 2022), p. 309.
5. I Putu Widiantara, Rosy Amalia Kurnia Putri, Da In Han, Warda Bahanan, Eun Hye Lee, Chang Hoon Woo, Jee-Hyun Kang, Jungho Ryu, and Young Gun Ko, *Materials*, **16**, Iss. 6: 2516 (2023).
6. S. Dong, G. Ma, P. Lei, T. Cheng, D. Savvakin, and O. Ivasishin, *Adv. Powder Technol.*, **32**, Iss. 7: 2300 (2021).
7. B. Wang, D. Savvakin, and O. Ivasishin, *Mater. Sci. Eng. A*, **808**: 140908 (2021).
8. *Materials Properties Handbook: Titanium Alloys* (Eds. R. Boyer, G. Welsh, and E. W. Collings) (ASM International: 1994).
9. www.polymim.com
10. O. M. Ivasishin, D. G. Savvakin, M. M. Gumenyak, and A. B. Bondarchuk, *Key Eng. Mater.*, **520**: 121 (2012).
11. M. Qian, *Int. J. Powder Metallurgy*, **46**, Iss. 5: 29 (2010).
12. O. M. Ivasishin, D. G. Savvakin, O. D. Rud, D. V. Oryshych, I. M. Kirian, A. M. Lakhnik, V. I. Bondarchuk, B. Kronowetter, Yu. I. Torba, and V. G. Manzhos, *Metallofiz. Noveishie Tekhnol.*, **47**, No. 4: 391 (2025).
13. D. Zuili, V. Maurice, and P. Marcus, *J. Electrochem. Soc.*, **147**: 1393 (2000).
14. X. Zhang, H. Deng, S. Xiao, Z. Zhang, J. Tang, L. Deng, and W. Hu, *J. Alloys Compd.*, **588**: 163 (2014).